nanomaterials

MDPI

Article

MOF-Derived Ultrathin Cobalt Molybdenum Phosphide Nanosheets for Efficient Electrochemical Overall Water Splitting

Xiang Wang [1,2], Linlin Yang [1,2], Congcong Xing [1], Xu Han [3], Ruifeng Du [1,2], Ren He [1,2], Pablo Guardia [1], Jordi Arbiol [3,4] and Andreu Cabot [1,4,*]

1 Catalonia Institute for Energy Research (IREC), Sant Adrià de Besòs, 08930 Barcelona, Spain; wxiang@irec.cat (X.W.); lyang@irec.cat (L.Y.); congcongxing@irec.cat (C.X.); ruifengdu@irec.cat (R.D.); renhe@irec.cat (R.H.); pguardia@irec.cat (P.G.)
2 Departament d'Enginyeria Electrònica i Biomèdica, Universitat de Barcelona, 08028 Barcelona, Catalonia, Spain
3 Catalan Institute of Nanoscience and Nanotechnology (ICN2), CSIC and BIST, Campus UAB, Bellaterra, 08193 Barcelona, Catalonia, Spain; xu.han@icn2.cat (X.H.); arbiol@icrea.cat (J.A.)
4 ICREA, Pg. Lluis Companys, 08010 Barcelona, Catalonia, Spain
* Correspondence: acabot@irec.cat

Abstract: The development of high-performance and cost-effective earth-abundant transition metal-based electrocatalysts is of major interest for several key energy technologies, including water splitting. Herein, we report the synthesis of ultrathin CoMoP nanosheets through a simple ion etching and phosphorization method. The obtained catalyst exhibits outstanding electrocatalytic activity and stability towards oxygen and hydrogen evolution reactions (OER and HER), with overpotentials down to 273 and 89 mV at 10 mA cm^{-2}, respectively. The produced CoMoP nanosheets are also characterized by very small Tafel slopes, 54.9 and 69.7 mV dec^{-1} for OER and HER, respectively. When used as both cathode and anode electrocatalyst in the overall water splitting reaction, CoMoP-based cells require just 1.56 V to reach 10 mA cm^{-2} in alkaline media. This outstanding performance is attributed to the proper composition, weak crystallinity and two-dimensional nanosheet structure of the electrocatalyst.

Keywords: MOF; phosphide; nanosheet; water splitting

Citation: Wang, X.; Yang, L.; Xing, C.; Han, X.; Du, R.; He, R.; Guardia, P.; Arbiol, J.; Cabot, A. MOF-Derived Ultrathin Cobalt Molybdenum Phosphide Nanosheets for Efficient Electrochemical Overall Water Splitting. *Nanomaterials* **2022**, *12*, 1098. https://doi.org/10.3390/nano12071098

Received: 9 March 2022
Accepted: 25 March 2022
Published: 27 March 2022

1. Introduction

Hydrogen, with a high gravimetric energy density (142 MJ kg^{-1}) and zero-carbon emissions, is both a key component in the chemical industry and a very appealing energy carrier for clean and sustainable energy storage and supply [1,2]. Since molecular hydrogen is not freely available in nature, it needs to be extracted from hydrogen-containing compounds. Currently, fossil fuels are the main source of H_2, which involves the release of large amounts of carbon. The electrochemical water splitting is the main green alternative to produce H_2, but it is seriously hampered by the high cost and insufficient durability of current electrocatalysts, based on scarce novel metals such as Pt, Ir and Ru [3–6], and the slow kinetics of the hydrogen and oxygen evolution reactions (HER, OER), which makes water electrolysis not competitive with steam reforming of natural gas or coal gasification processes [7–9].

In order to overcome the current challenges and enable the massive production of H_2 by water splitting, substantial efforts were devoted to the development of high activity, stable and cost-effective electrocatalysts for overall water splitting (OWS). Among the wide range of materials proposed for alkaline water electrolysis, including metal oxides/hydroxides [10–12], chalcogenides [13–16], nitrides [17,18] and carbides [19,20], metal phosphides demonstrated particularly attractive catalytic performances [21,22].

The outstanding performance of phosphides was related to their high electrical conductivity, favorable electronic structure and high stability against corrosion [23,24]. Amongst phosphides, cobalt phosphide (CoP) exhibits an exceptional HER activity associated with a proper electronic structure and specifically to the effective capture of protons by the negatively charged phosphorous atoms [25,26]. Besides, CoP is also characterized by a very high OER activity associated with the high ability of the positively charged cobalt cations to adsorb oxygen intermediates while the negatively-charged P facilitates the desorption of O_2 molecules [27,28]. However, the OWS in CoP still requires too large overpotentials for practical applications, mainly ascribed to the high dissociation energy of water and the sluggish OER kinetics involving a multi-electron transfer process [29,30].

An effective strategy to optimize a material's performance is the introduction of an additional element that provides additional degrees of freedom to modulate its electronic structure and surface properties. Within transition metal phosphide electrocatalysts, additional metals enable a fine-tuning of the d-band position, optimizing the adsorption free energy of the reactants/intermediates/products and thus improving the catalytic activity and even stability. In this direction, Xiao et al. reported the HER catalytic activity of CoP to be boosted by vanadium doping [31]. The introduced V strongly interacts with the hosted Co atoms, enhancing the VCoP electron density and thus accelerating the HER. Other elements, such as Zn [32], Mn [33], Ni [34], Ce [35], Cr [36] and W [21], were also demonstrated to promote either the HER or OER through enhancing electron interactions [28].

Beyond composition, the structure, morphology and organization of the catalyst particles are key parameters defining the density, accessibility and activity of the catalytic sites, which ultimately determine the catalytic activity. In this regard, metal–organic frameworks (MOFs), with a crystalline and porous structure formed by metal ion/cluster bridged by organic ligands, were demonstrated to be excellent sacrificial templates to produce porous carbon-based nanomaterials with tuned composition and morphology [37–40].

Inspired by the above considerations, we rationally designed a novel and highly effective bifunctional electrocatalyst for OWS. This new catalyst is based on CoP, structured as 2D ultrathin nanosheets and derived from the ZIF-67 MOF. It includes Mo^{6+} as a high valence 4d transition metal ion, which ionic radius of 0.62 Å matches well with that of Co^{3+} (0.63 Å), thus allowing the substitution of Co^{3+} by Mo^{6+} within the CoP lattice [41,42]. We demonstrated here that the proposed porous nanosheet-based structure and the incorporation of Mo within the CoP lattice enable rapid water dissociation and effective and stable HER and OER performances.

2. Materials and Methods

2.1. Chemicals

Ammonium molybdate tetrahydrate ($(NH_4)_6Mo_7O_{24}{\cdot}4H_2O$, 90%), cobalt nitrate hexahydrate ($Co(NO_3)_2{\cdot}6H_2O$, 99.9%), potassium hydroxide (KOH, 85%), iridium(IV) oxide (IrO_2, 99.9% metal basis) and Nafion (5 wt% within a blend of low aliphatic alcohols and water) were obtained from Sigma-Aldrich (St. Louis, MO, USA). 2-Methylimidazole ($C_4H_6N_2$, 99%) was purchased from Acros Organics (Antwerp, Belgium). Analytical grade methanol, ethanol and isopropanol were obtained from different sources. Milli-Q water was produced using an Elga Purelab flex. All chemicals were used as received.

2.2. Preparation of ZIF-67

ZIF-67 was produced following a previously reported procedure with some modifications [16,43]. Briefly, 0.87 g $Co(NO_3)_2{\cdot}6H_2O$ was dissolved in 30 mL of methanol to obtain a clear solution. Subsequently, the above solution was poured into 30 mL of methanol containing 1.97 g of 2-methylimidazole under vigorous stirring. After mixing completely, the solution was incubated for 24 h at room temperature. Purple precipitates were collected by centrifugation; they were washed with methanol three times and then dried at 60 °C overnight.

2.3. Preparation of Mo–Co MOFs

One hundred and twenty milligrams of as-prepared ZIF-67 powder was ultrasonically re-dispersed in 20 mL of ethanol. This solution was poured into 100 mL of an aqueous solution containing 50 mg, 100 mg and 200 mg of ammonium molybdate under continuous magnetic stirring. The mixture was then stirred vigorously for 24 h at room temperature. Lavender precipitates were collected by centrifugation, washed with water at least three times and freeze-dried overnight.

2.4. Preparation of CoP and CoMoP

The obtained ZIF-67 and Mo–Co MOFs powders were placed in a porcelain boat within a horizontal tube furnace. In another boat, a 20× mass amount of $NaH_2PO_2 \cdot H_2O$ was placed at the upstream side of the tube furnace. The material was then annealed at 350 °C under N_2 flow. After calcination for 2 h, the final black products were denoted as CoP and CoMoP, respectively.

2.5. Structural Characterization

Powder X-ray diffraction (XRD) was performed on a Bruker AXS D8 Advance X-ray diffractometer (Bruker, Billerica, MA, USA) with Cu-Kα radiation (λ = 1.5406 Å). Scanning electron microscopy (SEM) analysis was conducted with a Zeiss Auriga microscope (Carl Zeiss, Jena, Germany) equipped with an energy dispersive spectroscope analyses (EDS) detector operating at 20 kV. Transmission electron microscopy (TEM), High-resolution TEM (HRTEM), Annular dark-field scanning transmission electron microscope (HAADF-STEM) and electron energy loss spectroscopy (EELS) analysis were obtained using a field emission gun FEI Tecnai F20 microscope (FEI, Hillsboro, OR, USA) with a Gatan Quantum filter (Pleasanton, CA, USA) at 200 kV. X-ray photoelectron spectroscopy (XPS) measurements were conducted on a SPECS using an Al anode XR50 source at 150 W and a 150 MCD-9 detector from Phoibos (SPECS, Berlin, Germany).

2.6. Electrochemical Measurements

Electrochemical characterization was performed in a standard three-electrode system using an electrochemical workstation (CHI 760E, CH Instruments, Shanghai, China) in 1 M KOH solution (PH = 14). A graphite rod counter electrode and a Hg/HgO reference electrode were employed. Electrochemical impedance spectroscopy (EIS) was measured within a frequency from 0.01 Hz to 10 kHz at 10 mV amplitude. The initial voltage was fixed at the overpotential required to obtain a current density of 10 mA cm^{-2}. The electrochemically active surface area (ECSAs) was determined using the electrochemical double-layer capacitance (C_{dl}) obtained with cyclic voltammetry data at different scan rates (v = 20–100 $mV \cdot s^{-1}$). Stability was determined by CV using 3000 cycles at 100 $mV \cdot s^{-1}$ and by chronopotentiometry at 10 $mA \cdot cm^{-2}$. Overall water splitting tests were carried out in a two-electrode system with the voltage range of 0–2.0 V at a scan rate of 5 $mV \cdot s^{-1}$ in 1.0 M KOH electrolyte.

3. Results and Discussion

3.1. Characterization of Electrocatalysts

CoMoP nanosheets were produced by a three-step process involving the synthesis of a Co–MOF, its etching and partial cation exchange and a final phosphorization step, as schematically illustrated in Figure 1a. First, a cobalt-based zeolitic imidazolate framework (ZIF-67), consisting of polyhedral-shaped micrometer-size particles, was produced as a self-sacrificial template (Figure 1b). The ZIF-67 was reacted with ammonium molybdate with the double role of etching the structure and partially replacing Co^{3+} cations by Mo^{6+}, yielding a porous wrinkled nanosheet-based material that we refer to as Co–Mo MOF (Figure 1c). Finally, the Co–Mo MOF was annealed within a tube furnace containing NaH_2PO_2 at 350 °C for 2 h to produce a porous phosphide with a similar wrinkled nanosheet-based morphology that we denoted as CoMoP (Figures 1d and S1). EDS analysis

of CoMoP showed a Co–Mo atomic ratio of Co/Mo = 4, and a phosphorus–metal atomic ratio of P/M =2.6 (M = Co + Mo) (Figure S2).

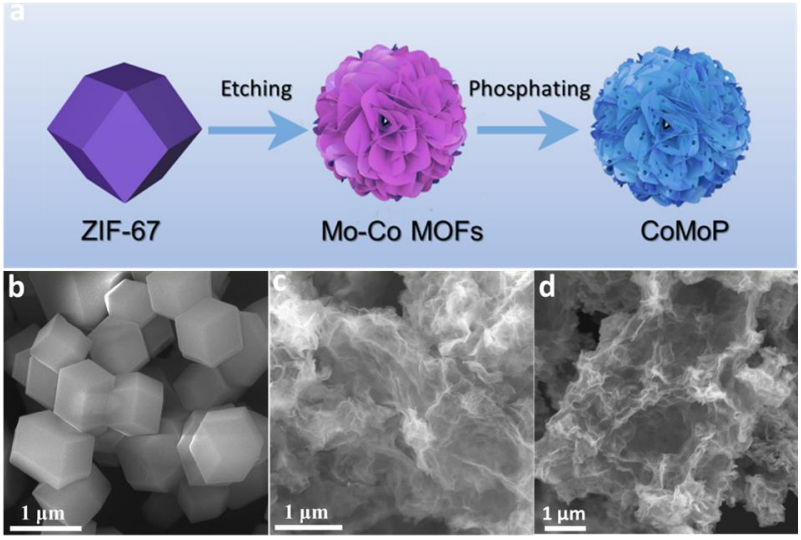

Figure 1. (**a**) Schematic illustration of the CoMoP synthesis process. (**b**–**d**) SEM image of (**b**) ZIF-67 (**c**) Mo–Co MOFs and (**d**) CoMoP.

In order to study the effect of ammonium molybdate, we replaced this chemical with an alternative Mo precursor. Using sodium molybdate as Mo source, the morphology of the final product was much more compact, consisting of partially porous cubes (Figure S3). Besides, EDS analysis revealed the molybdenum content of this material to be much lower (Co/Mo = 18.8) than that of CoMoP. We will refer to this material as Mo–CoP. As a reference, a Mo-free CoP was obtained by directly annealing the ZIF-67 in the presence of the phosphorous source, with no etching step (Figure S4). The obtained material also displayed a more compact geometry than that of the CoMoP nanosheets.

Figures 2a,b and S5 displays TEM images of CoMoP, further revealing their ultrathin nanosheet structure. HAADF-STEM analysis and EELS chemical composition maps (Figures 2e, S6 and S7) displayed a homogenous distribution of C, Co, Mo and P within each CoMoP nanosheet. HRTEM images (Figure 2c) and SAED patterns (Figure 2d) showed CoMoP to present a weak crystallinity, with strong middle/long-range disordered [44–46]. In this regard, while the XRD patterns of ZIF-67 and Na_2MoO_4-ZIF-67 displayed a good crystallinity (Figure 3a), the Co–Mo MOF already presented a mostly amorphous structure. After phosphorization, CoP maintained a relatively well-organized lattice, and CoMoP displayed a weak crystallographic order, consistently with HRTEM results (Figure 3b).

As expected, the XPS survey spectrum displayed the presence of C, N, O, P, Co and Mo elements on the surface of CoMoP (Figure 3c). The high-resolution P 2p XPS spectrum displayed two doublets, which we associated with P within the metal phosphide lattice (P $2p_{3/2}$ = 129.7 eV), and a phosphate chemical environment (P $2p_{3/2}$ = 133.8 eV) (Figure 3d) [41,47]. The Co 2p XPS spectrum displayed six peaks (Figure 3e). The main Co 2p contribution was assigned to Co within the phosphide lattice (Co $2p_{3/2}$ = 779.3 eV). A second doublet was associated with Co within an oxide, hydroxide or phosphate chemical environment (Co $2p_{3/2}$ = 781.5 eV). The last two bands were assigned to satellite peaks [28–30,48,49]. Finally, the Mo 3d XPS spectrum displayed two doublets assigned to Mo within the metal phosphide lattice (Mo $3d_{5/2}$ = 228.2 eV) and an oxidized chemical environment (Mo $3d_{5/2}$ = 233.0 eV) (Figure 3f) [50–52].

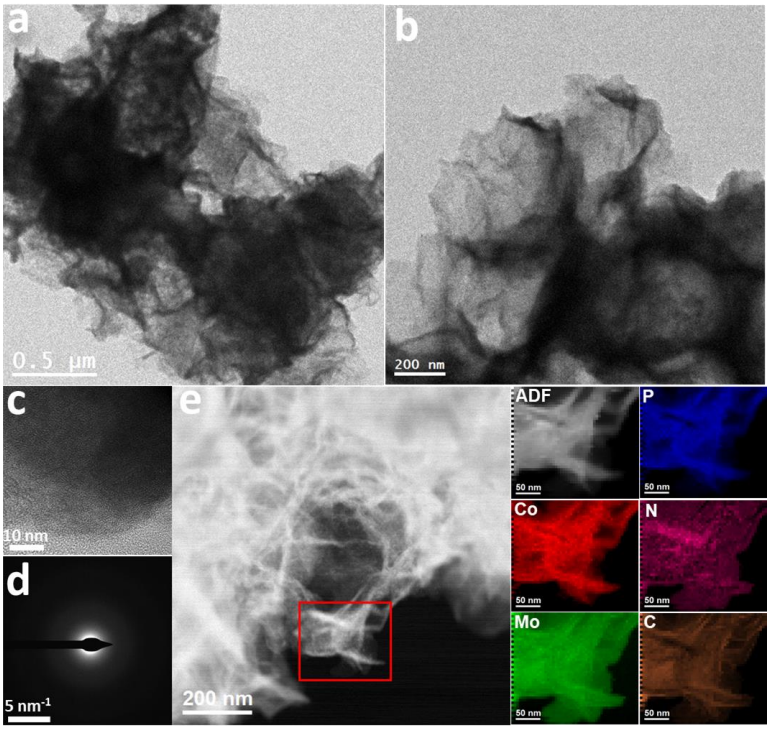

Figure 2. (**a**,**b**) TEM images, (**c**) HRTEM image, (**d**) SAED pattern and (**e**) HAADF STEM image and EELS chemical composition maps obtained from the red squared area of the STEM micrograph. Individual Co $L_{2,3}$ edges at 779 eV (red), Mo $M_{4,5}$ edges at 230 eV (green), P $L_{2,3}$ edges at 132 eV (blue), N K edge at 401 eV (pink) and C K edge at 284 eV (orange).

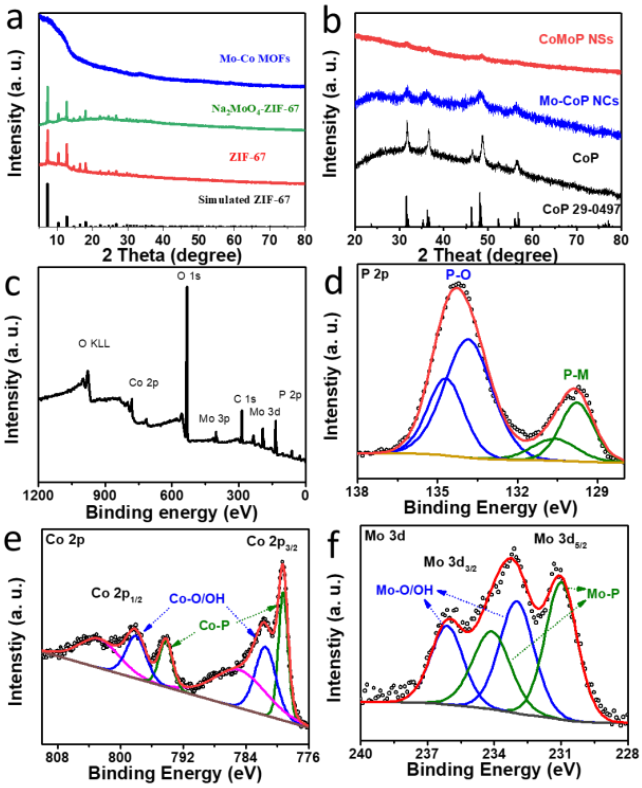

Figure 3. (**a**,**b**) XRD pattern of the MOFs (**a**) and the phosphorized materials, CoMoP, Mo–CoP and CoP. (**c**–**f**) XPS survey and high-resolution P 2p (**d**), Co 2p (**e**) and Mo 3d (**f**) XPS spectra of CoMoP.

3.2. Oxygen Evolution Reaction

The OER activity of CoMoP was evaluated at room temperature using a three-electrode system in a 1.0 M KOH alkaline solution. As a reference, Mo–CoP, CoP and a commercial RuO_2 catalyst were also evaluated in the same cell and reaction conditions. The LSV polarization curves displayed the CoMoP to be characterized by an outstanding OER activity, with an overpotential of only 273 mV at a current density of 10 mA cm^{-2} (Figures 4a and S8). This overpotential is well below that of Mo–CoP, CoP and the RuO_2 electrocatalyst tested here and outperforms that of previously reported CoP-based OER catalysts, as shown in Table S1. As displayed in Figure 4b, CoMoP was not only characterized by the lowest overpotential at 10 mA cm^{-2} but also provided the lowest Tafel slope, 54.9 mV dec^{-1}. This value was significantly below that of Mo–CoP (60.4 mV dec^{-1}), CoP (71.5 dec^{-1}) and RuO_2 (86.4 mV dec^{-1}), which indicates CoMoP to have associated a faster OER reaction kinetics [53,54].

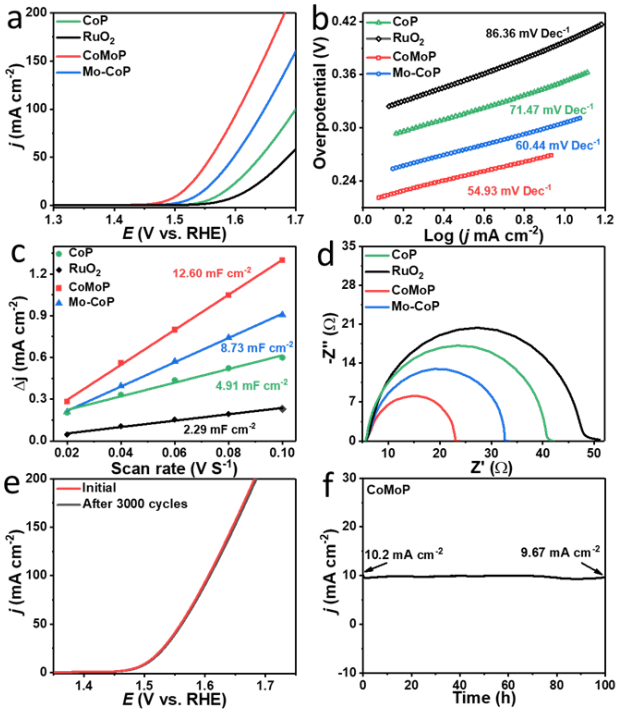

Figure 4. (**a**) OER polarization curves in 1.0 M KOH. (**b**) Corresponding Tafel plots. (**c**) Double-layer capacitances (C_{dl}). (**d**) Nyquist plots of the EIS data. (**e**) OER polarization curves before and after 3000 cycles. (**f**) OER chronoamperometric data for CoMoP at an overpotential of 273 mV.

The electrochemical active areas (ECSA) of CoMoP, Mo–CoP NCs, CoP and RuO_2 were estimated according to the double-layer capacitance (C_{dl}) determined via CV in the non-faradaic region at different scan rates, 20, 40, 60, 80 and 100 mV·s^{-1} (Figures S9 and 4c). CoMoP displayed larger C_{dl} (12.6 mF cm^{-2}) than Mo–CoP (8.7 mF cm^{-2}), CoP (4.9 mF cm^{-2}) and RuO_2 (2.3 mF cm^{-2}). This result indicates that CoMoP offers a higher density of accessible electrochemical active sites, which we relate to the proper composition and nanosheet structure of CoMoP.

The charge transport/transfer ability of the electrocatalysts was evaluated by electrochemical impedance spectroscopy (EIS). An equivalent circuit model including a charge transfer resistance (R_{ct}) and a solution resistance (R_s) during the OER process was used to fit the Nyquist plots displayed in Figure 4d [55,56]. CoMoP exhibited the smallest R_{ct} (17.99 Ω), well below that of Mo–CoP (R_{ct} = 27.90 Ω), CoP (R_{ct} = 36.70 Ω) and RuO_2 (45.47). These results reveal the CoMoP nanosheets to enable a faster charge transfer at the electrode/electrolyte interfaces, thus accelerating the OER electrocatalytic kinetics.

The long-term stability of CoMoP was further analyzed by CV and chronopotentiometry measurements [57,58]. Figure 4e shows how the LSV curve of CoMoP after 3000 CV

cycles closely resembles that of the first cycle. The chronoamperometry test displayed CoMoP to have an outstanding long-term catalytic activity with just a 3% current density decay after 100 h of operation at 273 mV (Figure 4f). SEM images of the post-catalysts after OER testing at high current showed the ultrathin CoMoP nanosheets to partially sinter into a highly porous structure with thicker walls (Figure S10). At the same time, the EDX result showed that a loss of P occurred during the OER. These results are consistent with the reorganization of the metal phosphide into a metal (oxy)-hydroxide during the OER reaction [59,60].

3.3. Hydrogen Evolution Reaction

The HER performance of CoMoP was evaluated in 1.0 M KOH using a three-electrode system, and it was compared with that of Mo–CoP, CoP and a commercial Pt/C catalyst. As shown in Figures 5a and S8b, the CoMoP electrocatalyst displayed a relatively low HER overpotential of 89 mV at the current density of 10 mA cm^{-2}, slightly above that of Pt/C (42 mV) and well below that of Mo–CoP (154 mV), CoP (165 mV) and most previously reported phosphide-based HER electrocatalysts (Table S2). The Tafel slope of CoMoP (69.7 mV dec^{-1}) was also much lower than those of Mo–CoP (83.7 mV dec^{-1}), CoP (113.4 mV dec^{-1}) and close to that of Pt/C (56.1 mV dec^{-1}) (Figure 5b), which indicated rapid HER reaction kinetics following the Volmer–Heyrovsky mechanism [61,62]. CoMoP also displayed the smallest semicircular diameter in the Nyquist plot of the EIS data among the phosphide catalysts tested (Figure 5c), showing the lowest charge transfer resistance during catalytic processes. In terms of stability under HER conditions, Figure 5d displays how CoMoP suffered a minor change in the LSV curves after 3000 cycles. Additionally, the CA measurement showed the current density to decrease just 6% after 100 h of continuous operation under HER conditions at an overpotential 89 mV (Figure 5e). The morphology and composition of the catalyst after long-term HER are displayed in Figure S11. In this case, minor changes in structure and a moderate P loss were observed, which points to notable catalyst stability under HER.

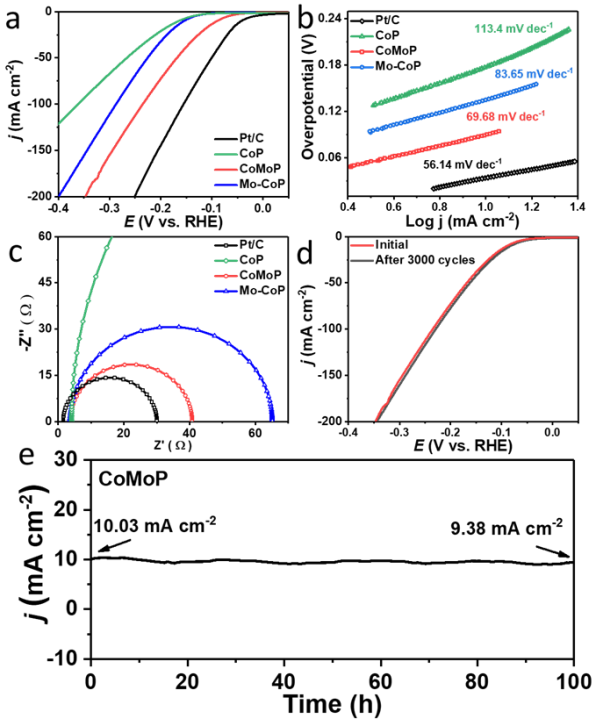

Figure 5. (**a**) HER polarization curves in 1.0 M KOH. (**b**) Corresponding Tafel plots. (**c**) Nyquist plots of the EIS data. (**d**) HER polarization curves before and after 3000 cycles. (**e**) Chronoamperometry data for CoMoP at a 89 mV overpotential.

3.4. Overall Water Splitting

Due to the excellent OER and HER performances demonstrated by CoMoP, a two-electrode configuration electrolyzer with CoMoP both as the positive and negative electrodes was constructed and tested for OWS in 1.0 M KOH solution (Figure 6a). As shown from the polarization curves displayed in Figure 6b, the assembled device just required a cell voltage of 1.56 V to reach a current density of 10 mA cm^{-2}, which is significantly below that of a cell containing Pt/C and RuO_2 electrodes (1.61 V). More importantly, after 40 h of continuous operation at 100 mA cm^{-2}, the CoMoP-based cell still maintained an outstanding performance, with just a 14.8% loss at high current density (Figure 6c). Thus, the as-prepared CoMoP can be considered as a highly competitive electrocatalytic catalyst for OWS compared with the previously reported OWS catalysts (Figure 6d, Table S3). Besides, its outstanding stability demonstrates its potential for large-scale hydrogen production from water splitting.

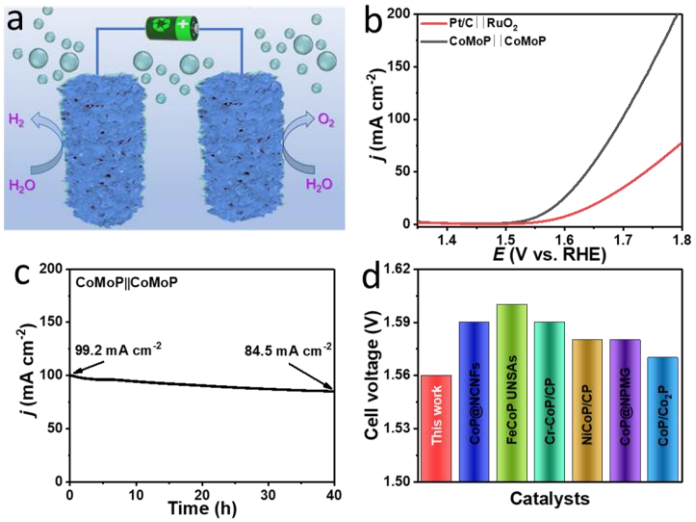

Figure 6. (**a**) Schematic diagram of the OWS in a two-electrode system. (**b**) Polarization curves of OWS cells with the electrode pairs: CoMoP||CoMoP and Pt/C||RuO_2 in 1.0 M KOH. (**c**) Chronoamperometric curve of CoMoP in the two-electrode system at 1.70 V polarization. (**d**) Comparison of the CoMoP overpotential at 10 mA cm^{-2} with previously reported catalysts in 1.0 M KOH.

4. Conclusions

In conclusion, ultrathin CoMoP nanosheets were engineered using the Co–MOF ZIF-67 as a self-sacrificial template and ammonium molybdate as a shape-defining agent and Mo source. CoMoP nanosheets exhibited outstanding performance towards HER and OER in alkaline media, which we associate with the proper transport properties and electronic energy levels provided by their composition and their porous nanosheet structure. In particular, CoMoP presented low overpotentials of 89 and 273 mV at a current density of 10 mA cm^{-2} for HER and OER, respectively. Furthermore, CoMoP electrocatalysts also showed excellent long-term stabilities in alkaline electrolytes, with a minor current density decrease after 100 h continuous operation. When used for OWS, a cell voltage of only 1.56 V was needed to reach a current density of 10 mA cm^{-2}. This work provides a suitable strategy to synthesize high-performance Co–Mo–P electrocatalysts with abundant exposed active sites and effective avenues for charge and electrolyte transport, and it can be employed to further tune the structure and composition of other 2D nanostructures with optimized performance towards OWS and other electrocatalytic reactions.

Supplementary Materials: The following supporting information can be downloaded at: https://www.mdpi.com/article/10.3390/nano12071098/s1, Figure S1: (a–f) SEM images of CoMoP; Figure S2: (a) SEM images of Co–Mo MOFs. (b,c) SEM images and (d) EDX spectrum of CoMoP. Figure S3: (a) SEM images of Na2MoO4-ZIF-67. (b,c) SEM images and (d) EDX spectrum Mo–CoP.; Figure S4:

(a) SEM images of ZIF-67. (b,c) SEM images and d) EDX spectrum CoP. Figure S5: (a–d) TEM image of CoMoP. Figure S6: (a–d) HAADF-STEM micrographs of CoMoP. Figure S7: EELS chemical composition maps obtained from the red squared area of the STEM micrograph. Individual Co L2,3-edges at 779 eV (red), Mo M4,5-edges at 230 eV (green), P L2,3-edges at 132 eV (blue), N K-edge at 401 eV (pink) and C K-edge at 284 eV (orange). Figure S8: (a) OER and (b) HER polarization curves of CoMoP with different Mo content in 1.0 M KOH. Figure S9: Cyclic voltammograms for (a) CoMoP; (b) Mo–CoP; (c) CoP and (d) RuO2 in the non-faradaic region of 1.12–1.22 V vs. RHE at various scan rates. Figure S10: (a–c) SEM image and (d) EDX spectrum of CoMoP after long-term OER stability testing. Figure S11: (a–c) SEM image and (d) EDX spectrum of CoMoP after long-term HER stability testing. Table S1: Comparison of OER performance of CoMoP with some previously reported CoP-based catalysts in 1.0 M KOH solution. Table S2: Comparison of HER performance of CoMoP with some previously reported CoP-based catalysts in 1.0 M KOH solution. Table S3: Comparison of OWS performance of CoMoP with some previously reported CoP-based catalysts in 1.0 M KOH solution. References [63–81] are cited in the supplementary materials.

Author Contributions: The manuscript was prepared through the contribution of all authors. A.C. guided the project and supervised the work. X.W., L.Y., C.X., R.D., R.H. and P.G. conceived and prepared the manuscript. X.W. and L.Y. produced the samples. X.W. and C.X. performed the electrochemical measurements and analyzed the results. X.H., J.A. and P.G. performed TEM, HRTEM and discussed these results. X.W. and R.H. performed XPS measurements and discussed these results. The manuscript was corrected and improved by all authors. All authors have read and agreed to the published version of the manuscript.

Funding: This research was partially funded by the project Combenergy, PID2019-105490RB-C32, from the Spanish Ministerio de Ciencia e Innovación. X.W., L.Y., C.X., X.H. and R.D. thank the China Scholarship Council (CSC) for the scholarship support. IREC is funded by the CERCA Programme/Generalitat de Catalunya. Part of the present work has been performed in the frameworks of Universitat de Barcelona Nanoscience Ph.D. program. ICN2 acknowledges funding from Generalitat de Catalunya 2017 SGR 327. The authors thank the support from the project NANOGEN (PID2020-116093RB-C43), funded by MCIN/AEI/10.13039/501100011033/. ICN2 is supported by the Severo Ochoa program from Spanish MINECO (Grant No. SEV-2017-0706) and is funded by the CERCA Programme/Generalitat de Catalunya. Part of the present work has been performed in the framework of Universitat Autònoma de Barcelona Materials Science Ph.D. program.

Data Availability Statement: The data are available on reasonable request from the corresponding authors.

Conflicts of Interest: The authors declare no conflict of interest.

References

1. Zou, X.; Zhang, Y. Noble metal-free hydrogen evolution catalysts for water splitting. *Chem. Soc. Rev.* **2015**, *44*, 5148–5180. [CrossRef] [PubMed]
2. Zhu, J.; Hu, L.; Zhao, P.; Lee, L.Y.S.; Wong, K.Y. Recent Advances in Electrocatalytic Hydrogen Evolution Using Nano-particles. *Chem. Rev.* **2020**, *120*, 851–918. [CrossRef] [PubMed]
3. Zhang, L.; Jang, H.; Liu, H.; Kim, M.G.; Yang, D.; Liu, S.; Liu, X.; Cho, J. Sodium-Decorated Amorphous/Crystalline RuO_2 with Rich Oxygen Vacancies: A Robust pH-Universal Oxygen Evolution Electrocatalyst. *Angew. Chem. Int. Ed.* **2021**, *60*, 18821–18829. [CrossRef] [PubMed]
4. Chen, Z.; Duan, X.; Wei, W.; Wang, S.; Ni, B.-J. Iridium-based nanomaterials for electrochemical water splitting. *Nano Energy* **2020**, *78*, 105270. [CrossRef]
5. Ruiz Esquius, J.; Algara-Siller, G.; Spanos, I.; Freakley, S.J.; Schlögl, R.; Hutchings, G.J. Preparation of Solid Solution and Layered IrOx–$Ni(OH)_2$ Oxygen Evolution Catalysts: Toward Optimizing Iridium Efficiency for OER. *ACS Catal.* **2020**, *10*, 14640–14648. [CrossRef]
6. Yu, T.; Xu, Q.; Qian, G.; Chen, J.; Zhang, H.; Luo, L.; Yin, S. Amorphous CoOx-Decorated Crystalline RuO_2 Nanosheets as Bifunctional Catalysts for Boosting Overall Water Splitting at Large Current Density. *ACS Sustain. Chem. Eng.* **2020**, *8*, 17520–17526. [CrossRef]
7. Cao, L.; Luo, Q.; Liu, W.; Lin, Y.; Liu, X.; Cao, Y.; Zhang, W.; Wu, Y.; Yang, J.; Yao, T.; et al. Identification of single-atom active sites in carbon-based cobalt catalysts during electrocatalytic hydrogen evolution. *Nat. Catal.* **2019**, *2*, 134–141. [CrossRef]
8. Chung, D.Y.; Lopes, P.P.; Martins, P.F.B.D.; He, H.; Kawaguchi, T.; Zapol, P.; You, H.; Tripkovic, D.; Strmcnik, D.; Zhu, Y.; et al. Dynamic stability of active sites in hydr(oxy)oxides for the oxygen evolution reaction. *Nat. Energy* **2020**, *5*, 222–230. [CrossRef]
9. McKone, J.R.; Marinescu, S.C.; Brunschwig, B.S.; Winkler, J.R.; Gray, H.B. Earth-abundant hydrogen evolution electro-catalysts. *Chem. Sci.* **2014**, *5*, 865–878. [CrossRef]

10. Badreldin, A.; Abusrafa, A.E.; Abdel-Wahab, A. Oxygen-Deficient Cobalt-Based Oxides for Electrocatalytic Water Splitting. *ChemSusChem* **2021**, *14*, 10–32. [CrossRef]
11. Bigiani, L.; Barreca, D.; Gasparotto, A.; Andreu, T.; Verbeeck, J.; Sada, C.; Modin, E.; Lebedev, O.I.; Morante, J.R.; Maccato, C. Selective anodes for seawater splitting via functionalization of manganese oxides by a plasma-assisted process. *Appl. Catal. B Environ.* **2021**, *284*, 119684. [CrossRef]
12. Xiao, Z.; Wang, Y.; Huang, Y.-C.; Wei, Z.; Dong, C.-L.; Ma, J.; Shen, S.; Li, Y.; Wang, S. Filling the oxygen vacancies in Co3O4with phosphorus: An ultra-efficient electrocatalyst for overall water splitting. *Energy Environ. Sci.* **2017**, *10*, 2563–2569. [CrossRef]
13. Joo, J.; Kim, T.; Lee, J.; Choi, S.; Lee, K. Morphology-Controlled Metal Sulfides and Phosphides for Electrochemical Water Splitting. *Adv. Mater.* **2019**, *31*, e1806682. [CrossRef] [PubMed]
14. Zhu, X.; Dai, J.; Li, L.; Zhao, D.; Wu, Z.; Tang, Z.; Ma, L.-J.; Chen, S. Hierarchical carbon microflowers supported defect-rich Co_3S_4 nanoparticles: An efficient electrocatalyst for water splitting. *Carbon* **2020**, *160*, 133–144. [CrossRef]
15. Tan, L.; Yu, J.; Wang, H.; Gao, H.; Liu, X.; Wang, L.; She, X.; Zhan, T. Controllable synthesis and phase-dependent catalytic performance of dual-phase nickel selenides on Ni foam for overall water splitting. *Appl. Catal. B Environ.* **2021**, *303*, 120915. [CrossRef]
16. Wang, X.; Li, F.; Li, W.; Gao, W.; Tang, Y.; Li, R. Hollow bimetallic cobalt-based selenide polyhedrons derived from metal–organic framework: An efficient bifunctional electrocatalyst for overall water splitting. *J. Mater. Chem. A* **2017**, *5*, 17982–17989. [CrossRef]
17. Jia, J.-R.; Zhai, M.-K.; Lv, J.-J.; Zhao, B.-X.; Du, H.; Zhu, J.-J. Nickel Molybdenum Nitride Nanorods Grown on Ni Foam as Efficient and Stable Bifunctional Electrocatalysts for Overall Water Splitting. *ACS Appl. Mater. Interfaces* **2018**, *10*, 30400–30408. [CrossRef]
18. Lu, Y.; Li, Z.; Xu, Y.; Tang, L.; Xu, S.; Li, D.; Zhu, J.; Jiang, D. Bimetallic Co-Mo nitride nanosheet arrays as high-performance bifunctional electrocatalysts for overall water splitting. *Chem. Eng. J.* **2021**, *411*, 128433. [CrossRef]
19. Yu, Y.; Zhou, J.; Sun, Z. Novel 2D Transition-Metal Carbides: Ultrahigh Performance Electrocatalysts for Overall Water Splitting and Oxygen Reduction. *Adv. Funct. Mater.* **2020**, *30*, 2000570. [CrossRef]
20. Yang, C.; Zhao, R.; Xiang, H.; Wu, J.; Zhong, W.; Li, W.; Zhang, Q.; Yang, N.; Li, X. Ni-Activated Transition Metal Carbides for Efficient Hydrogen Evolution in Acidic and Alkaline Solutions. *Adv. Energy Mater.* **2020**, *10*, 2002260. [CrossRef]
21. Lu, S.-S.; Zhang, L.-M.; Dong, Y.-W.; Zhang, J.-Q.; Yan, X.-T.; Sun, D.-F.; Shang, X.; Chi, J.-Q.; Chai, Y.-M.; Dong, B. Tungsten-doped Ni–Co phosphides with multiple catalytic sites as efficient electrocatalysts for overall water splitting. *J. Mater. Chem. A* **2019**, *7*, 16859–16866. [CrossRef]
22. Pu, Z.; Zhao, J.; Amiinu, I.S.; Li, W.; Wang, M.; He, D.; Mu, S. A universal synthesis strategy for P-rich noble metal di-phosphide-based electrocatalysts for the hydrogen evolution reaction. *Energy Environ. Sci.* **2019**, *12*, 952–957. [CrossRef]
23. Song, J.; Zhu, C.; Xu, B.Z.; Fu, S.; Engelhard, M.H.; Ye, R.; Du, D.; Beckman, S.P.; Lin, Y. Bimetallic Cobalt-Based Phosphide Zeo-litic Imidazolate Framework: CoPxPhase-Dependent Electrical Conductivity and Hydrogen Atom Adsorption Energy for Effi- cient Overall Water Splitting. *Adv. Energy Mater.* **2017**, *7*, 1601555. [CrossRef]
24. Shi, Y.; Zhang, B. Recent advances in transition metal phosphide nanomaterials: Synthesis and applications in hydrogen evolution reaction. *Chem. Soc. Rev.* **2016**, *45*, 1529–1541. [CrossRef]
25. Hou, C.; Zou, L.; Wang, Y.; Xu, Q. Frontispiece: MOF-Mediated Fabrication of a Porous 3D Superstructure of Carbon Nanosheets Decorated with Ultrafine Cobalt Phosphide Nanoparticles for Efficient Electrocatalysis and Zinc–Air Batteries. *Angew. Chem. Int. Ed.* **2020**, *59*, 21360–21366. [CrossRef] [PubMed]
26. Xu, W.; Fan, G.; Zhu, S.; Liang, Y.; Cui, Z.; Li, Z.; Jiang, H.; Wu, S.; Cheng, F. Electronic Structure Modulation of Nanoporous Cobalt Phosphide by Carbon Doping for Alkaline Hydrogen Evolution Reaction. *Adv. Funct. Mater.* **2021**, *31*, 2107333. [CrossRef]
27. Zhi, L.; Tu, J.; Li, J.; Li, M.; Liu, J. 3D holey hierarchical nanoflowers assembled by cobalt phosphide embedded N-doped carbon nanosheets as bifunctional electrocatalyst for highly efficient overall water splitting. *J. Colloid Interface Sci.* **2022**, *616*, 379–388. [CrossRef]
28. Zhao, Y.; Zhang, J.; Xie, Y.; Sun, B.; Jiang, J.; Jiang, W.-J.; Xi, S.; Yang, H.Y.; Yan, K.; Wang, S.; et al. Constructing Atomic Heterometallic Sites in Ultrathin Nickel-Incorporated Cobalt Phosphide Nanosheets via a Boron-Assisted Strategy for Highly Efficient Water Splitting. *Nano Lett.* **2021**, *21*, 823–832. [CrossRef]
29. Dutta, S.; Indra, A.; Han, H.; Song, T. An Intriguing Pea-Like Nanostructure of Cobalt Phosphide on Molybdenum Car-bide Incorporated Nitrogen-Doped Carbon Nanosheets for Efficient Electrochemical Water Splitting. *ChemSusChem* **2018**, *11*, 3956–3964. [CrossRef]
30. Chai, L.; Hu, Z.; Wang, X.; Xu, Y.; Zhang, L.; Li, T.T.; Hu, Y.; Qian, J.; Huang, S. Stringing Bimetallic Metal-Organic Frame-work-Derived Cobalt Phosphide Composite for High-Efficiency Overall Water Splitting. *Adv. Sci.* **2020**, *7*, 1903195. [CrossRef]
31. Xiao, X.; Tao, L.; Li, M.; Lv, X.; Huang, D.; Jiang, X.; Pan, H.; Wang, M.; Shen, Y. Electronic modulation of transition metal phosphide via doping as efficient and pH-universal electrocatalysts for hydrogen evolution reaction. *Chem. Sci.* **2018**, *9*, 1970–1975. [CrossRef] [PubMed]
32. Liu, T.; Liu, D.; Qu, F.; Wang, D.; Zhang, L.; Ge, R.; Hao, S.; Ma, Y.; Du, G.; Asiri, A.M.; et al. Enhanced Electrocatalysis for Energy-Efficient Hydrogen Production over CoP Catalyst with Nonelectroactive Zn as a Promoter. *Adv. Energy Mater.* **2017**, *7*, 1700020. [CrossRef]
33. Liu, T.; Ma, X.; Liu, D.; Hao, S.; Du, G.; Ma, Y.; Asiri, A.M.; Sun, X.; Chen, L. Mn doping of CoP nanosheets array: An efficient electrocatalyst for hydrogen evolution reaction with enhanced activity at all pH values. *ACS Catal.* **2017**, *7*, 98–102. [CrossRef]

34. Xiao, X.; He, C.-T.; Zhao, S.; Li, J.; Lin, W.; Yuan, Z.; Zhang, Q.; Wang, S.; Dai, L.; Yu, D. A general approach to cobalt-based homobimetallic phosphide ultrathin nanosheets for highly efficient oxygen evolution in alkaline media. *Energy Environ. Sci.* **2017**, *10*, 893–899. [CrossRef]
35. Gao, W.; Yan, M.; Cheung, H.-Y.; Xia, Z.; Zhou, X.; Qin, Y.; Wong, C.-Y.; Ho, J.C.; Chang, C.-R.; Qu, Y. Modulating electronic structure of CoP electrocatalysts towards enhanced hydrogen evolution by Ce chemical doping in both acidic and basic media. *Nano Energy* **2017**, *38*, 290–296. [CrossRef]
36. Wu, Y.; Tao, X.; Qing, Y.; Xu, H.; Yang, F.; Luo, S.; Tian, C.; Liu, M.; Lu, X. Cr-Doped FeNi–P Nanoparticles Encapsulated into N-Doped Carbon Nanotube as a Robust Bifunctional Catalyst for Efficient Overall Water Splitting. *Adv. Mater.* **2019**, *31*, e1900178. [CrossRef]
37. Wang, H.-F.; Chen, L.; Pang, H.; Kaskel, S.; Xu, Q. MOF-derived electrocatalysts for oxygen reduction, oxygen evolution and hydrogen evolution reactions. *Chem. Soc. Rev.* **2020**, *49*, 1414–1448. [CrossRef]
38. Xu, H.; Cao, J.; Shan, C.; Wang, B.; Xi, P.; Liu, W.; Tang, Y. MOF-Derived Hollow CoS Decorated with CeOx Nanoparticles for Boosting Oxygen Evolution Reaction Electrocatalysis. *Angew. Chem. Int. Ed.* **2018**, *57*, 8654–8658. [CrossRef]
39. Wang, W.; Yan, H.; Anand, U.; Mirsaidov, U. Visualizing the Conversion of Metal–Organic Framework Nanoparticles into Hollow Layered Double Hydroxide Nanocages. *J. Am. Chem. Soc.* **2021**, *143*, 1854–1862. [CrossRef]
40. Yang, B.; Du, Y.; Shao, M.; Bin, D.; Zhao, Q.; Xu, Y.; Liu, B.; Lu, H. MOF-derived RuCoP nanoparticles-embedded nitro-gen-doped polyhedron carbon composite for enhanced water splitting in alkaline media. *J. Colloid Interface Sci.* **2022**, *616*, 803–812. [CrossRef]
41. Tang, Y.-J.; Zhu, H.-J.; Dong, L.-Z.; Zhang, A.M.; Li, S.-L.; Liu, J.; Lan, Y.-Q. Solid-phase hot-pressing of POMs-ZIFs precursor and derived phosphide for overall water splitting. *Appl. Catal. B* **2019**, *245*, 528–535. [CrossRef]
42. Teng, Y.; Gao, J.-X.; Li, J.-Y.; Chen, H.-Y.; Wang, X.-D.; Kuang, D.-B. Engineering multinary heterointerfaces in two-dimensional cobalt molybdenum phosphide hybrid nanosheets for efficient electrocatalytic water splitting. *Sustain. Energy Fuels* **2021**, *5*, 3458–3466. [CrossRef]
43. Wang, X.; Huang, X.; Gao, W.; Tang, Y.; Jiang, P.; Lan, K.; Yang, R.; Wang, B.; Li, R. Metal–organic framework derived $CoTe_2$ encapsulated in nitrogen-doped carbon nanotube frameworks: A high-efficiency bifunctional electrocatalyst for overall water splitting. *J. Mater. Chem. A* **2018**, *6*, 3684–3691. [CrossRef]
44. Anantharaj, S.; Noda, S. Amorphous Catalysts and Electrochemical Water Splitting: An Untold Story of Harmony. *Small* **2020**, *16*, e1905779. [CrossRef]
45. Huang, H.; Cho, A.; Kim, S.; Jun, H.; Lee, A.; Han, J.W.; Lee, J. Structural Design of Amorphous CoMoPx with Abundant Active Sites and Synergistic Catalysis Effect for Effective Water Splitting. *Adv. Funct. Mater.* **2020**, *30*, 2003889. [CrossRef]
46. Qian, Q.; Li, Y.; Liu, Y.; Zhang, G. General anion-exchange reaction derived amorphous mixed-metal oxides hollow na-noprisms for highly efficient water oxidation electrocatalysis. *Appl. Catal. B* **2020**, *266*, 118642. [CrossRef]
47. Wang, Z.; Wei, C.; Zhu, X.; Wang, X.; He, J.; Zhao, Y. A hierarchical carbon nanotube forest supported metal phosphide electrode for efficient overall water splitting. *J. Mater. Chem. A* **2020**, *9*, 1150–1158. [CrossRef]
48. Wu, J.; Wang, D.; Wan, S.; Liu, H.; Wang, C.; Wang, X. An Efficient Cobalt Phosphide Electrocatalyst Derived from Cobalt Phosphonate Complex for All-pH Hydrogen Evolution Reaction and Overall Water Splitting in Alkaline Solution. *Small* **2020**, *16*, e1900550. [CrossRef]
49. Yan, L.; Zhang, B.; Zhu, J.; Li, Y.; Tsiakaras, P.; Kang Shen, P. Electronic modulation of cobalt phosphide nanosheet arrays via copper doping for highly efficient neutral-pH overall water splitting. *Appl. Catal. B* **2020**, *265*, 118555. [CrossRef]
50. Han, Y.; Li, P.; Tian, Z.; Zhang, C.; Ye, Y.; Zhu, X.; Liang, C. Molybdenum-Doped Porous Cobalt Phosphide Nanosheets for Efficient Alkaline Hydrogen Evolution. *ACS Appl. Energy Mater.* **2019**, *2*, 6302–6310. [CrossRef]
51. Wei, Y.; Li, W.; Li, D.; Yi, L.; Hu, W. Amorphous-crystalline cobalt-molybdenum bimetallic phosphide heterostructured nanosheets as Janus electrocatalyst for efficient water splitting. *Int. J. Hydrog. Energy* **2021**, *47*, 7783–7792. [CrossRef]
52. Yu, L.; Xiao, Y.; Luan, C.; Yang, J.; Qiao, H.; Wang, Y.; Zhang, X.; Dai, X.; Yang, Y.; Zhao, H. Cobalt/Molybdenum Phosphide and Oxide Heterostructures Encapsulated in N-Doped Carbon Nanocomposite for Overall Water Splitting in Alkaline Media. *ACS Appl. Mater. Interfaces* **2019**, *11*, 6890–6899. [CrossRef] [PubMed]
53. Chen, H.; Chen, J.; Ning, P.; Chen, X.; Liang, J.; Yao, X.; Chen, D.; Qin, L.; Huang, Y.; Wen, Z. 2D Heterostructure of Amor-phous CoFeB Coating Black Phosphorus Nanosheets with Optimal Oxygen Intermediate Absorption for Improved Electro-catalytic Water Oxidation. *ACS Nano* **2021**, *15*, 12418. [CrossRef] [PubMed]
54. Gu, L.F.; Chen, J.J.; Zhou, T.; Lu, X.F.; Li, G.R. Engineering cobalt oxide by interfaces and pore architectures for enhanced electrocatalytic performance for overall water splitting. *Nanoscale* **2020**, *12*, 11201–11208. [CrossRef]
55. Huang, L.; Chen, D.; Luo, G.; Lu, Y.R.; Chen, C.; Zou, Y.; Dong, C.L.; Li, Y.; Wang, S. Zirconium-Regulation-Induced Bi-functionality in 3D Cobalt-Iron Oxide Nanosheets for Overall Water Splitting. *Adv. Mater.* **2019**, *31*, e1901439. [CrossRef]
56. Niu, S.; Jiang, W.J.; Wei, Z.; Tang, T.; Ma, J.; Hu, J.S.; Wan, L.J. Se-Doping Activates FeOOH for Cost-Effective and Efficient Electrochemical Water Oxidation. *J. Am. Chem. Soc.* **2019**, *141*, 7005–7013. [CrossRef]
57. Chen, Z.; Zhang, T.; Gao, X.; Huang, Y.; Qin, X.; Wang, Y.; Zhao, K.; Peng, X.; Zhang, C.; Liu, L.; et al. Engineering Microdomains of Oxides in High-Entropy Alloy Electrodes toward Efficient Oxygen Evolution. *Adv. Mater.* **2021**, *33*, 2101845. [CrossRef]
58. Duan, Y.; Lee, J.Y.; Xi, S.; Sun, Y.; Ge, J.; Ong, S.J.H.; Chen, Y.; Dou, S.; Meng, F.; Diao, C.; et al. Anodic Oxidation Enabled Cation Leaching for Promoting Surface Reconstruction in Water Oxidation. *Angew. Chem. Int. Ed.* **2021**, *60*, 7418–7425. [CrossRef]

59. Jin, S. Are Metal Chalcogenides, Nitrides, and Phosphides Oxygen Evolution Catalysts or Bifunctional Catalysts? *ACS Energy Lett.* **2017**, *2*, 1937–1938. [CrossRef]
60. Chu, H.; Feng, P.; Jin, B.; Ye, G.; Cui, S.; Zheng, M.; Zhang, G.-X.; Yang, M. In-situ release of phosphorus combined with rapid surface reconstruction for Co–Ni bimetallic phosphides boosting efficient overall water splitting. *Chem. Eng. J.* **2021**, *433*, 133523. [CrossRef]
61. Ma, H.; Chen, Z.; Wang, Z.; Singh, C.V.; Jiang, Q. Interface Engineering of Co/CoMoN/NF Heterostructures for High-Performance Electrochemical Overall Water Splitting. *Adv. Sci.* **2022**, 2105313. [CrossRef] [PubMed]
62. Jin, J.; Yin, J.; Liu, H.; Huang, B.; Hu, Y.; Zhang, H.; Sun, M.; Peng, Y.; Xi, P.; Yan, C.H. Atomic Sulfur Filling Oxygen Vacancies Optimizes H Absorption and Boosts the Hydrogen Evolution Reaction in Alkaline Media. *Angew. Chem. Int. Ed.* **2021**, *60*, 14117–14123. [CrossRef] [PubMed]
63. Zhou, G.; Li, M.; Li, Y.L.; Dong, H.; Sun, D.; Liu, X.; Xu, L.; Tian, Z.; Tang, Y. Regulating the electronic structure of CoP nanosheets by O incorporation for high-efficiency electrochemical overall water splitting. *Adv. Funct. Mater.* **2019**, *30*, 1905252. [CrossRef]
64. Pan, Y.; Sun, K.; Liu, S.; Cao, X.; Wu, K.; Cheong, W.-C.; Chen, Z.; Wang, Y.; Li, Y.; Liu, Y.; et al. Core–Shell ZIF-8@ZIF-67-Derived CoP Nanoparticle-Embedded N-Doped Carbon Nanotube Hollow Polyhedron for Efficient Overall Water Splitting. *J. Am. Chem. Soc.* **2018**, *140*, 2610–2618. [CrossRef] [PubMed]
65. Guan, C.; Xiao, W.; Wu, H.; Liu, X.; Zang, W.; Zhang, H.; Ding, J.; Feng, Y.P.; Pennycook, S.J.; Wang, J. Hollow Mo-doped CoP nanoarrays for efficient overall water splitting. *Nano Energy* **2018**, *48*, 73–80. [CrossRef]
66. Saad, A.; Shen, H.; Cheng, Z.; Ju, Q.; Guo, H.; Munir, M.; Turak, A.; Wang, J.; Yang, M. Three-Dimensional Mesoporous Phosphide–Spinel Oxide Heterojunctions with Dual Function as Catalysts for Overall Water Splitting. *ACS Appl. Energy Mater.* **2020**, *3*, 1684–1693. [CrossRef]
67. Zhang, M.; Ci, S.; Li, H.; Cai, P.; Xu, H.; Wen, Z. Highly defective porous CoP nanowire as electrocatalyst for full water splitting. *Int. J. Hydrogen Energy* **2017**, *42*, 29080–29090. [CrossRef]
68. Xie, X.-Q.; Liu, J.; Gu, C.; Li, J.; Zhao, Y.; Liu, C.-S. Hierarchical structured CoP nanosheets/carbon nanofibers bifunctional electrocatalyst for high-efficient overall water splitting. *J. Energy Chem.* **2021**, *64*, 503–510. [CrossRef]
69. Hei, J.C.; Xu, G.C.; Wei, B.; Zhang, L.; Ding, H.; Liu, D.J. NiFeP nanosheets on N-doped carbon sponge as a hierarchically structured bifunctional electrocatalyst for efficient overall water splitting. *Appl. Surf. Sci.* **2021**, *549*, 149297. [CrossRef]
70. Shuai, C.; Mo, Z.L.; Niu, X.H.; Zhao, P.; Dong, Q.B.; Chen, Y.; Liu, N.J.; Guo, R.B. Nickel/cobalt bimetallic phosphides derived metal-organic frameworks as bifunctional electrocatalyst for oxygen and hydrogen evolution reaction. *J. Alloys Compd.* **2020**, *847*, 156514. [CrossRef]
71. Liu, G.; Shuai, C.; Mo, Z.; Guo, R.; Liu, N.; Niu, X.; Dong, Q.; Wang, J.; Gao, Q.; Chen, Y.; et al. The one-pot synthesis of porous $Ni_{0.85}Se$ nanospheres on graphene as an efficient and durable electrocatalyst for overall water splitting. *New J. Chem.* **2020**, *44*, 17313–17322. [CrossRef]
72. Zhang, C.-L.; Xie, Y.; Liu, J.-T.; Cao, F.-H.; Cong, H.-P.; Li, H. 1D Core−Shell MOFs derived CoP Nanoparticles-Embedded N-doped porous carbon nanotubes anchored with MoS2 nanosheets as efficient bifunctional electrocatalysts. *Chem. Eng. J.* **2021**, *419*, 129977. [CrossRef]
73. Li, J.; Zou, S.; Liu, X.; Lu, Y.; Dong, D. Electronic Modulation of CoP by Ce Doping as Highly Efficient Electrocatalysts for Water Splitting. *ACS Sustain. Chem. Eng.* **2020**, *8*. [CrossRef]
74. Qin, J.-F.; Lin, J.-H.; Chen, T.-S.; Liu, D.-P.; Xie, J.-Y.; Guo, B.-Y.; Wang, L.; Chai, Y.-M.; Dong, B. Facile synthesis of V-doped CoP nanoparticles as bifunctional electrocatalyst for efficient water splitting. *J. Energy Chem.* **2019**, *39*, 182–187. [CrossRef]
75. Zhou, L.; Shao, M.; Li, J.; Jiang, S.; Wei, M.; Duan, X. Two-dimensional ultrathin arrays of CoP: Electronic modulation toward high performance overall water splitting. *Nano Energy* **2017**, *41*, 583–590. [CrossRef]
76. Li, W.; Jiang, Y.; Li, Y.; Gao, Q.; Shen, W.; Jiang, Y.; He, R.; Li, M. Electronic modulation of CoP nanoarrays by Cr-doping for efficient overall water splitting. *Chem. Eng. J.* **2021**, *425*, 130651. [CrossRef]
77. Yang, L.; Liu, R.M.; Jiao, L.F. Electronic redistribution: Construction and modulation of interface engineering on CoP for enhancing overall water splitting. *Adv. Funct. Mater.* **2020**, *30*, 1909618. [CrossRef]
78. Liang, H.; Gandi, A.N.; Anjum, D.H.; Wang, X.; Schwingenschlögl, U.; Alshareef, H.N. Plasma-Assisted Synthesis of NiCoP for Efficient Overall Water Splitting. *Nano Lett.* **2016**, *16*, 7718–7725. [CrossRef]
79. Liu, Z.; Yu, X.; Xue, H.; Feng, L. A nitrogen-doped CoP nanoarray over 3D porous Co foam as an efficient bifunctional electrocatalyst for overall water splitting. *J. Mater. Chem. A* **2019**, *7*, 13242–13248. [CrossRef]
80. Liu, Y.; Zhu, Y.; Shen, J.; Huang, J.; Yang, X.; Li, C. CoP nanoparticles anchored on N,P-dual-doped graphene-like carbon as a catalyst for water splitting in non-acidic media. *Nanoscale* **2018**, *10*, 2603–2612. [CrossRef]
81. Hua, Y.; Xu, Q.; Hu, Y.; Jiang, H.; Li, C. Interface-strengthened CoP nanosheet array with Co_2P nanoparticles as efficient electrocatalysts for overall water splitting. *J. Energy Chem.* **2018**, *37*, 1–6. [CrossRef]